Iraqi Journal of Physics, 2019 *Vol.17, No.40, PP. 95-107*

DOI: 10.20723/ijp.17.40.95-107

Structural and optical properties of Fe- doped ZnO thin films prepared by Sol–Gel spin coating process and their photocatalytic activities

Selma M. H. Al-Jawad[1], Sabah H. Sabeeh[1], Hussein A. Jassim[1], Natheer Jamal Imran[2]

[1]Applied Sciences Department, University of Technology, Baghdad, Iraq

[2]Ministry of Science and Technology, Iraq

E-mail: 100069@uotechnology.edu.iq

Abstract

Pure and Fe-doped zinc oxide nanocrystalline films were prepared via a sol–gel method using spin coating process. Pure and Fe-doped zinc oxide, containing 2 to 8 % Fe, were annealed at 500℃ for 2 h. The thin films were prepared and characterized by X-ray diffraction (XRD), atomic force microscopy (AFM), field emission scanning electron microscopy (FE-SEM) and UV- visible spectroscopy. The XRD results showed that ZnO has hexagonal wurtzite structure and the Fe ions were well incorporated into the ZnO structure. As the Fe level increased from 2 wt% to 8 wt%, the crystallite size reduced in comparison with the pure ZnO. The transmittance spectra were then recorded at wavelengths ranging from 300 nm to 1000 nm. The optical band gap energy of spin-coated films also decreased as Fe doping concentration increased. In particular, their optical band gap energies were 3.75, 3.6, 3.5, 3.45 and 3.3 eV doping concentration of 0%, 2%, 4%, 6% and 8% Fe, respectively. The performance of the pure and doped ZnO thin films was examined for the photocatalytic activity using organic dyes (methyl orange, methyl blue, methyl violet). The samples ZnO with concentration of Fe showed increased photocatalytic activity with an optimal maximum performance at 0.8 wt%.

Key words

Zinc oxide thin films spin coating, photocatalytic activities.

Article info.

Received: Sep. 2018
Accepted: Nov. 2018
Published: Mar. 2019

دراسة الخصائص التركيبية والبصرية للأغشية الرقيقة النانوية ZnO المشوبة بالحديد المحضرة بواسطة طريقة محلول-جيلاتين وانشطتها بالتحفيز الضوئي

سلمى محمد حسين الجواد[1] ، صباح حبيب صبيح[1]، حسين علي جاسم[1]، نذير جمال عمران[2]

[1]قسم العلوم التطبيقية، الجامعة التكنولوجية، بغداد، العراق

[2]وزارة العلوم والتكنولوجيا، العراق

الخلاصة

تم تحضير اغشية رقيقة لأوكسيد الزنك النقي و المشوبة بالحديد بواسطة طريقة محلول-جيلاتين. تم تلدين اغشية أوكسيد الزنك النقي و المشوبة التي تحتوي على 2 الى 8٪ من الحديد في درجة حرارة 500 درجة مئوية لمدة ساعتين. تم دراسة جميع الاغشية المحضرة باستخدام جهاز حيود الأشعة السينية (XRD)، مجهر القوة الذرية (AFM)، مجال الماسح الضوئي المجهر الإلكتروني (FESEM) ومطياف الطيف المرئي-الأشعة فوق البنفسجية. اظهرت نتائج حيود الاشعة السينية أن أغشية اوكسيد الزنك النقية والمشوبة له هيكل wurtzite

سداسي وقد تم دمج أيونات الحديد بشكل جيد في بنية ZnO. وتبين كذلك ان الحجم البلوري يقل بزيادة تركيز الاشابة بالحديد من 2 ٪ إلى 8 ٪wt ، انخفض حجم البللورات مقارنةً بـ ZnO النقي. ثم تم تسجيل أطياف النفاذية عند أطوال موجية تتراوح بين 300 نانومتر إلى 1000 نانومتر. قد اظهرت نتائج قياس فجوة الطاقة البصرية انها تقل بزيادة تركيز الاشابة بالحديد حيث تراوحت قيم فجوة الطاقة 3.75 و 3.6 و 3.5 و 3.45 و 3.3 الكترون-فولت عند تركيز الاشابة 0٪ و 2٪ و 4٪ و 6٪ و 8٪ على التوالي. تم فحص أداء الأغشية الرقيقة ZnO النقية والمشوبة للنشاط التحفيزي باستخدام الصبغات العضوية (برتقالي الميثيل، ميثيل الأزرق، ميثيل البنفسج). وأظهرت عينات ZnO مع تركيز Fe زيادة النشاط التحفيزي مع أقصى قدر من الأداء الأمثل في 0.8 wt ٪.

Introduction

Zinc oxide (ZnO) is a semiconductor compound of the II-VI family, with wide and direct band gap of (3.37 eV) [1] and large exiton binding energy (60 meV) at room temperature in the ultraviolet (UV) range abundant in nature, nontoxic and environmental friendly photocatalyst [2]. It has high catalytic efficiency with low cost, so that is one of the most widely used photocatalysts. |Because the intrinsic defects prevailing in materials, has effective in modulating the activity of the photocatalyst [3]. For example, some authors examined that introduction of surface oxygen vacancies in ZnO was an effective way to produce visible response and enhance photocatalytic activity [4-6]. Many process such as dopant, higher temperature annealed [4, 7] were used to make defects and then improve the photocatalytic activity. It is usually agreeable that surface defects are useful to the photocatalytic activity [8]. In addition, zinc oxide has high defect and many forms of defects occur in ZnO thin films such as oxygen vacancy and zinc vacancy [9]. At first the crystallite size of ZnO nanocrystalline is decide the properties of ZnO. Where, the presence of the defects can it altered structure properties of ZnO [10]. The ZnO photocatalyst thin films must be absorb not only ultraviolet radiation but also visible light, to achieve better photocatalytic efficiency in many applications [11]. To absorb visible light of solar spectrum, the energy band gap should be decreased by doping [12].

Many methods, such as hydrothermal method [13], sol-gel method [14], plasma-enhanced chemical vapor deposition (PECVD) [15], rf-magnetron sputtering [16], electro spinning [17] and so on are used to produce ZnO or doped ZnO thin films [18]. Among these techniques, the sol–gel method is attractive because of its simplicity, capability to produce good-quality films at a large scale, lower crystallization temperature, safe operation, low cost of equipment, and easy adjusting composition and dopants.

In this study, Fe:ZnO thin films were deposited and characterized through sol–gel spin coating. The photocatalytic activities of these films were also evaluated as a function of doping concentration and enhanced.

Experimental

1. ZnO preparation

Twenty five ml of methanol was mixed with 25 ml isopropanol (IPA), a 1.0975 g of zinc acetate was added to prepare 0.1M of ZnO seed solutions. The mixtures were vigorously stirred at 60 $^{\circ}$C for 1 h. Subsequently, monoethanolamine (MEA) was added drop wise to the solution under constant stirring at 60 $^{\circ}$C for 12 h, which was used as a stabilizer. Different molar concentration (2 %, 4 %, 6 %, and 8 %) of ferric nitrate as dopant was dissolved in the ZnO sol after the reagent was thoroughly

mixed. The solution was aged at room temperature for 24 h prior to the deposition process, where a transparent and homogenous solution was obtained. ZnO gel was deposited on the glass substrate by using spin coating method. Then, the films were dried at 150 °C for twenty min and annealed at 500 °C for 2 h.

2. Characterization of nanocrystalline ZnO Fe-doped films

The crystal structure of ZnO films was analyzed using X-ray diffraction (XRD) system (Shimadzu X-ray diffraction) with CuKα1 radiation at λ=1.54 Å.

From Scherrer–Debye formula, was calculated the average crystallite size [19]

$D= 0.9\ \lambda /\beta\cos\theta$ (nm) (1)

where k = 0.94, λ =1.54060 Å, β = Full Width Half Maximum (FWHM) and θ= Diffracting angle.

Also was calculated the micro-strain from the relation [20]:

$$\varepsilon = \frac{|a_{JCPD} - a_{XRD}|}{a_{JCPD}} * 100\% \quad (2)$$

Film thickness was measured by interferometry Fizeau using a He–Ne laser (0.632 μm). The morphologies of the resulting films were characterized by atomic force microscopy (AFM) (CSPM-5000) and scanning electron microscopy (SEM) (VEGA TE Scan). The optical transmittance and absorbance measurement were performed with UV/Vis spectrophotometer (UV-1800 Shimadzu) with double beam at a wavelength range from 300–1000 nm.

3. Photocatalytic degradation of organic dyes

The photocatalytic activity of pure and Fe-doped ZnO samples was determined from the degradation of methyl orange (MO), methyl blue (MB) and methyl violet (MV) were chosen as the target compounds during its catalytic decomposition. The MO, MB and MV are organic water soluble dyes found in waste waters and are potentially toxic.

Photocatalytic experiments were carried out in reactor of a static cylindric flask of 500 mL, coated by aluminum foil. The photodegradation reactor was equipped with two lamps TUV 6W G6 T8 quartz lamps, placed lamps on reactor. Each of the two lamps emitted a broad range of UV light, of λ_{max} = 254 nm.

Was measured value initial concentration of (MO), (MB) and (MV) before irradiation and then measure concentration of (MO), (MB) and (MV) at each interval of time after irradiation. The pure and Fe-doped ZnO coated slides were immersed in the dyes solution, and stirring under a magnetic stirrer. The samples were exposed to illumination up to 60 minutes for each sample in the dyes solution, the reaction was maintained at room temperature. Period the pure and Fe-doped ZnO thin films were irradiated with two lamps 6W (UV) light source with central wavelength emission at 254 nm. Furthermore, in each typical catalytic run, the dyes solution of catalyst free was illuminated under the same reaction conditions and was used as a control. No significant decrease in dyes concentration observed after UV light exposure in the absence of catalyst. This indicates that the photochemical degradation was negligible under UV-A irradiation with low energy. The absorbance of (MO), (MB) and (MV) solutions was supervised at periods of 15 min and monitored photocatalytic degradation of methyl orange (MO), methyl blue (MB) and methyl violet (MV) using UV–Vis spectrophotometer (UV-1800 Shimadzu) with double beam at a wavelength range from 300–1000 nm. After 60 min of irradiation, the

absorbance is registered at λ_{max} that is 460 nm for methyl orange (MO), 660 nm for methyl blue (MB) and 560 nm for methyl violet (MV) respectively. The concentration of the dyes solutions were 100 mg/L.

Results and discussion

1. XRD analysis

The X-ray diffraction analysis for thin films of zinc oxide in various Fe-doping levels, namely 0, 2, 4, 6 and 8 wt. %, are shown in Fig.1. All thin films are polycrystalline, with hexagonal wurtzite ZnO structure, and the peak positions of the films were found to be in good agreement with the established standards (JCPDS No. 36-1451). An XRD patterns was achieved to study the orientation and crystal quality of the deposited pure and ZnO with different doping concentrations thin films (Fig. 1). Based on Fig.1, the crystal growth orientation of pure and Fe doped with 2 % thin film has preferential growth along (101) and (100) planes, followed by (002), (110), (103), (102) and (112). It was observed that, by increasing the Fe doping concentration, the intensity of all diffraction peaks occurs in general. An addition to, the intensity of all the diffraction peaks was found decreasing with increasing Fe doping concentration. This caused by the formation of the stresses resulting from the effects of disorders or defects created by the Fe ions in the ZnO lattice structure [21], or because the kinetics of crystal growth has effected by chemical reactivity of the dopant [22], due to the low chemical reactivity of the iron in the zinc oxide lattice compared to the zinc, adding iron into ZnO lattice decreased the crystal growth speed and hence the crystallite sizes. This result is matches with the results of other authors, Mahmoudi et al. [21], ZnO nanoparticles doped with Fe were prepared by sol-gel method using $Fe(NO_3)_3.9H_2O$ as the dopant and X-ray diffraction results exhibited that the higher concentration of Fe doping give rise weakening of crystalline which is identical to our experimental result. Wang et al. [23] were deposited ZnO doped with Fe on glass and Silicon substrates by using magnetron sputtering method, XRD results exhibited that the FWHM increased and the intensity of diffraction peak decreased with increasing iron doping content, showing that the crystalline quality of ZnO thin film decrease gradually. However, the results are very various for other authors with other growth techniques and dopant sources Salaken et al. [24].

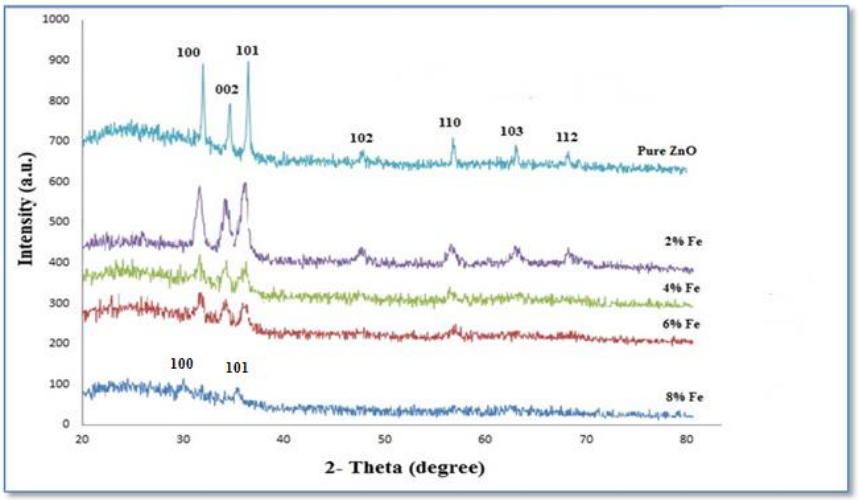

Fig. 1: XRD pattern of ZnO thin films for different doping concentrations of Fe.

2. Effect of iron doping on crystallite size

The crystallite size of ZnO thin films was calculated by using Eq. (1) as shown in Fig.2. The sizes of the zinc oxide crystallite, which was calculated to be 31.23, 11.08, 9.98, 9.90, and 9.53 nm, correspond to the peak of (101) plane, with a Fe doping in solution of 0, 2, 4, 6 and 8 wt% respectively. As shown, increased Fe concentration decreases the average crystallite size, and this behavior is caused by the increase in strain as a result of the increase in Fe concentration as shown in Fig.3 was calculated using equation. This result is in good agreement with [25].

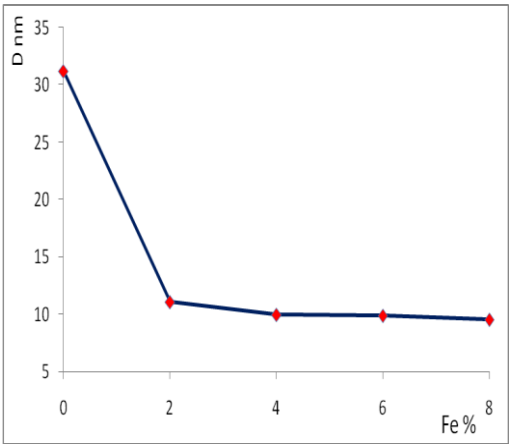

Fig.2: The variation of crystallite size (D) for ZnO thin film with Fe doping concentrations.

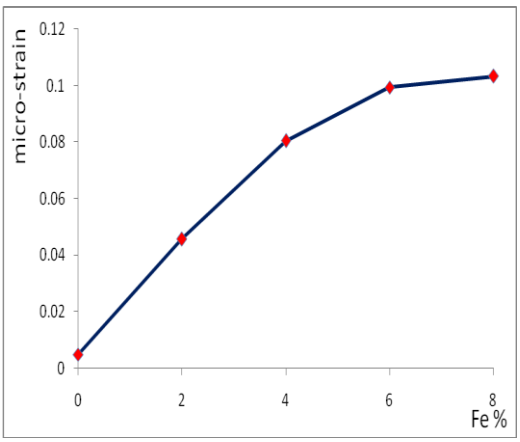

Fig. 3: The variation of micro-strain (ε) for ZnO thin film with Fe doping concentrations.

3. Effect of iron doping on lattice parameters

The increasing doping concentration lead to decrease of all the lattice constants (a=b, c) of the thin film as shown in Fig.4. Shows all the lattice constants, had decreased value compared with pure ZnO film. These reducing was attributed to the ionic radius of Zn^{2+} is larger than that of Fe^{3+}, suggesting that when Fe^{3+} replaces Zn^{2+} in the lattice substitutionally, it results in a smaller lattice constants of doped films than that of pure ZnO film [26].

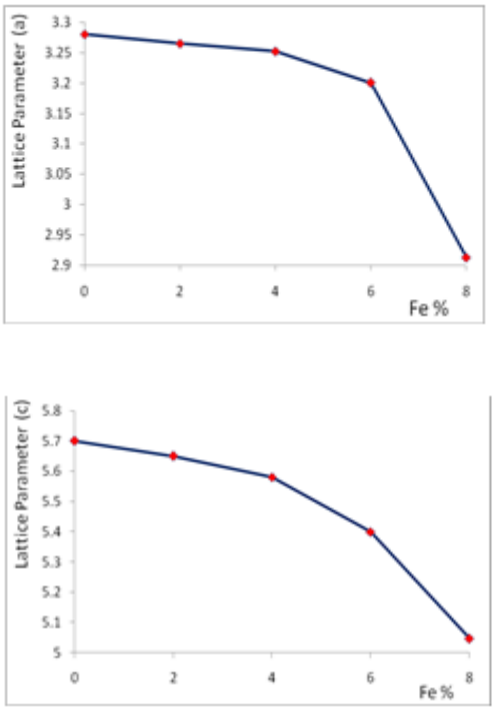

Fig.4: The variation of Lattice parameter for ZnO thin film with Fe doping concentrations.

4. Effect of iron doping on diffraction peak angle of XRD

Fig.5 shows the relation between differection angle of (101) peak with Fe doping concentration. From figure we observed that the (101) peak position was shifted to the lower angle with increasing doping concentration. A similar result is also reported by Mahmoudi et al. [21]. While, the researchers Salaken et al.[24]

exhibited that the (101) peak the considerable shifts towards higher angle direction with the increase of doping level. The solubility of the dopant depends on the ionic radius and the valence states. In Fe doped ZnO thin films, for maintaining charge neutrality, Fe ions need to have a valence of +2 in order to substitute Zn^{2+} ionic sites. When adding Fe in the ZnO lattice, for holding charge neutrality, the lattice structure are expected to deform by the Fe^{3+} ions [26]. And taking into consideration the ionic radii, the ionic radius of Zn^{2+}, Fe^{2+} and Fe^{3+} are 0.074, 0.078 and 0.068 nm, respectively. Thus, the ionic radius of Zn^{2+} is larger than Fe^{3+} by 8.1%, whereas that of Zn^{2+} is smaller than that of Fe^{2+} by 5.4%. Due to the difference of ionic radii between Fe^{2+} and Fe^{3+} so that both will result in different types and magnitudes of strain, when Fe^{2+} and Fe^{3+} substitute lattice sites in site of Zn^{2+} substitutionally. If Fe substitute lattice sites in site of Zn^{2+} substitutionally in the form Fe^{2+}, due to Zn^{2+} has smaller ionic radius than that of Fe^{2+}, it will lead to compression strain in the film [27], so that the peaks of XRD is shifting towards smaller angle direction (as shown in our experimental and by researchers Mahmoudi et al.[21]). And if Fe substitute lattice sites in site of Zn^{2+} substitutionally in the form Fe^{3+}, due to Zn^{2+} has larger ionic radius than that of Fe^{3+}, it will lead to tensile strain in the film, so that the peaks of XRD is shifting towards larger angle direction (as shown by the researchers Salaken et al.).

When Fe ions occur in ZnO mainly in the form of Fe^{2+}, due to its larger ionic radius of Fe^{2+} than that of Zn^{2+}, it will produce to compression strain in the film [27]. A visualization of this situation in XRD patterns is shifting of the peak towards smaller angle direction. On the contrary, if Fe ions occur in ZnO mainly in the form of Fe^{3+}, due to its smaller ionic radius than that of Zn^{2+}, it will lead to tensile strain in the film, producing a shifting of the peak towards bigger angle direction in XRD patterns.

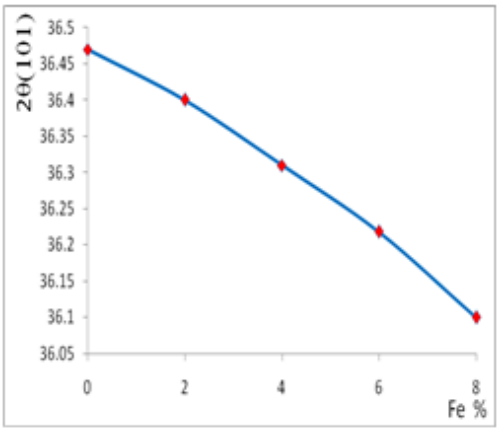

Fig.5 : The variation of 2θ (101) for ZnO thin film with Fe doping concentrations.

5. Morphological analysis

Fig.6 reveals the 3D and cumulating distribution AFM images of pure ZnO thin films doped with 2, 4, 6 and 8 % Fe concentrations. The average grain size, which is measured from AFM analysis using software, of doped and nondoped synthesized ZnO films ranged from 100 nm to 72 nm. AFM results show that adding Fe to ZnO thin films causes the films to become rough and porous and have a small grain size. This result is in good agreement with [22]. Table 1 shows the grain size, roughness values, and root mean square of ZnO thin films.

Fig.7 shows the field emission scanning electron microscopy (FE-SEM) images displaying the top view of the ZnO thin films for pure and doping with 4% on glass substrate. The FE-SEM images clearly illustrate the formation of flake-like nano-sized crystallite with more or less uniform structure of ZnO. The morphology of the films appears to be due to the growth and clustering of initial nuclei.

Doped films have randomly oriented and distinct flake shape structure. These results are in agreement with that of previous studies [24]. The SEM image with low magnification of ZnO film shows smooth ganglia-like hills (Fig.5).

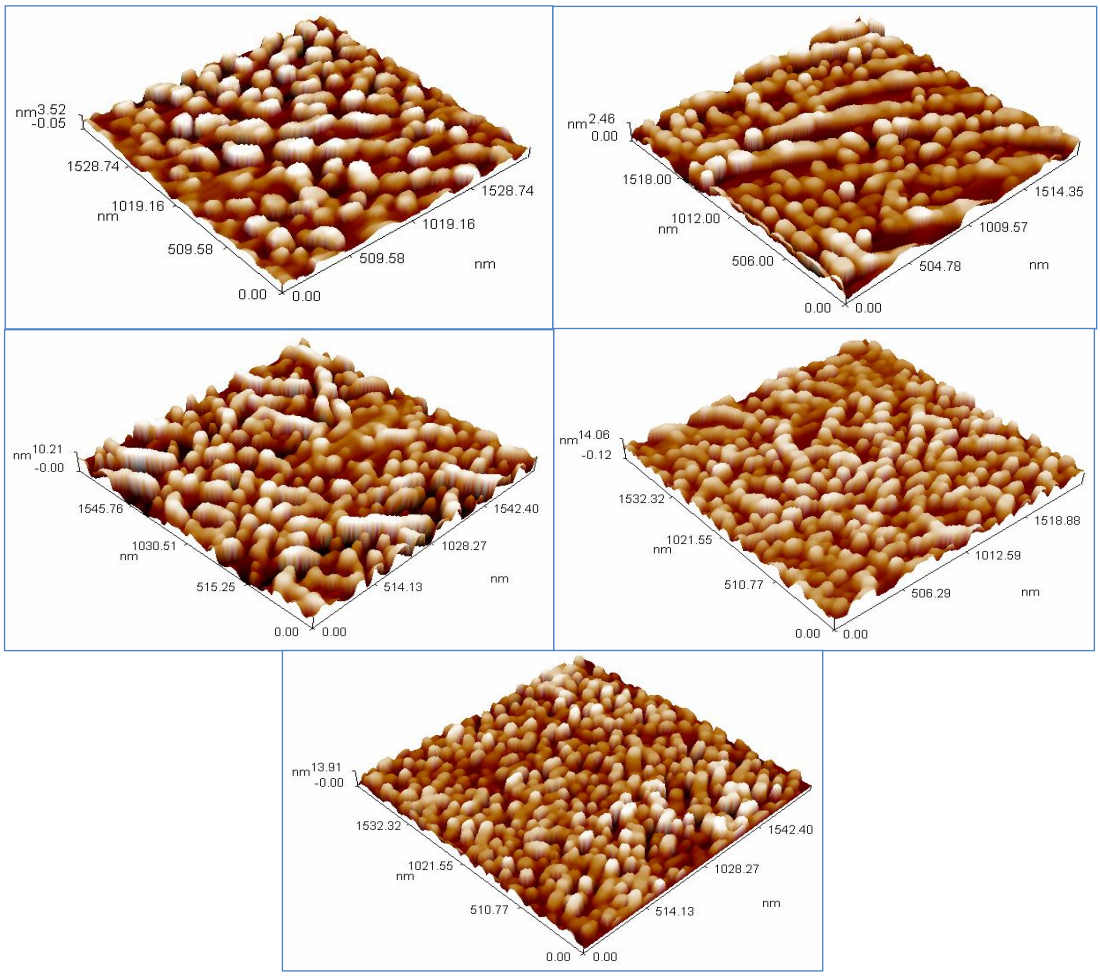

Fig.6 : AFM Images for pure and Fe-doped ZnO films (A) Pure ZnO (B) Fe-ZnO 2% (C) Fe-ZnO 4 % (D) Fe- ZnO 6% (E) Fe- ZnO 8 %.

Table 1: Grain size and root mean square of surface obtained from AFM data.

No.	Thin films	Grain size (nm)	Root Mean Square S_q (nm)	Roughness Average Sa (nm)
1	Pure ZnO	100	0.982	0.85
2	2% Fe - ZnO	96	2.98	2.63
3	4% Fe - ZnO	84	2.92	2.52
4	6% Fe - ZnO	82	2.72	2.36
5	8% Fe - ZnO	72	3.24	2.71

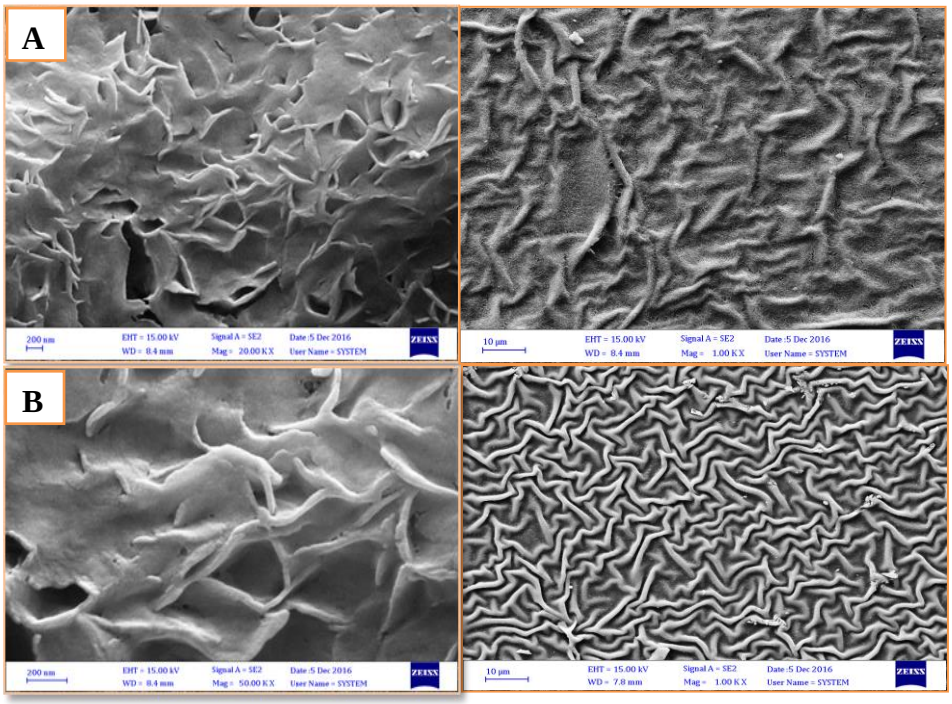

Fig.7: The FE-SEM image (top view) of ZnO thin films: (A) Pure ZnO (B) Fe- ZnO 4 %.

6. Optical analysis

The band gaps of thin films are calculated using the following equation [28]:

$$\alpha h\upsilon = A\,(h\upsilon - Eg)^{r} \qquad (3)$$

where α is the coefficient of absorption, h is the Planck's constant, Eg is the optical energy band gap of the material, υ is the frequency of light, r is the factor controlling the direct and indirect translation of the electrons from the valence band to the conduction band, *A* is constant, and hν is the energy of photon. Fig. 8 shows the relationship between $(\alpha\ h\nu)^2$ and energy of photon *hν*. The results indicate that an increase in the Fe content from 0 % to 8 wt. % leads to a decrease in the energy band gap from 3.75 eV to 3.3 eV, as shown in Fig.8 This reduction in energy gap is caused by the presence of prohibited impurities that led to the formation of donor levels within the energy gap near the conduction band. These results are in agreement with those of [29]. Interestingly, to achieve better photocatalytic efficiency, band gap energy of pure and Fe-doped zinc oxide thin films photocatalysts must have to be decreased [11].

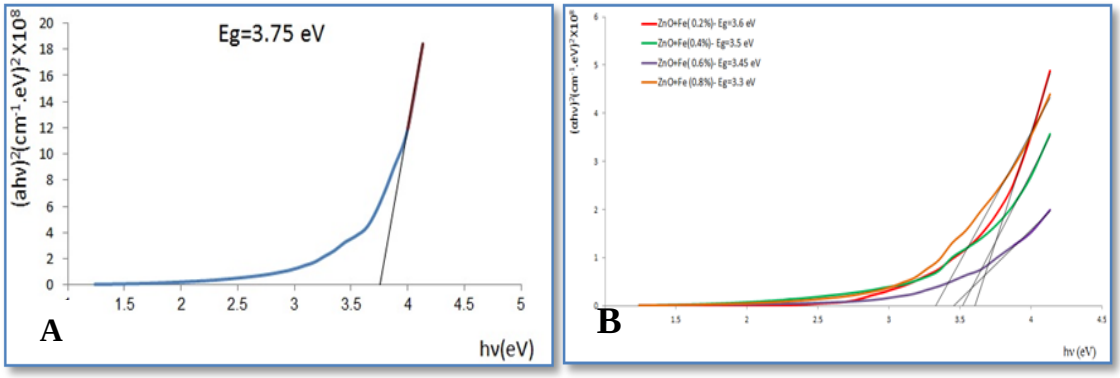

Fig.8: $(\alpha h\nu)^2$ versus photon energy plot of (A) pure ZnO thin films (B) with different doping concentration of Fe.

Photocatalytic activity

The photoreactivity of semiconductor is very sensitive to the morphology, crystal structure, phase composition and shape [30]. Also, the photocatalytic efficiency depends on the band structure, the electronic interaction between semiconductor and adsorbates, and the adsorption dynamics of substrate and intermediates [30]. The reaction is initiated by absorption of light with energy equal or higher than the energy band gap and the generation of electron hole pair on ZnO surface. The methyl orange (MO), methyl blue (MB) and methyl violet (MV) reacts with electrons produced on the zinc oxide thin films under UV irradiation. The technicality of the photocatalytic activity has been illustrated elsewhere [31]. Fig. 9 shows the absorbance spectra of the (a) methyl orange (MO) at 460 nm, (b) methyl blue (MB) at 660 nm and (c) methyl violet (MV) at 560 nm as a function of irradiation time on the zinc oxide for pure and doped thin films immersed in the dyes solution. It was concentration of the solutions were 100 mg/L. In order to confirm the photocatalytic activity, the spectrum was recorded at various time periods. The test was reduplicated with three sets of thin films at similar conditions and the results were reproducible.

Fig.9 shows the absorbance decreases with irradiation time, which suggests the photocatalytic activity of methyl orange (MO), methyl blue (MB) and methyl violet (MV). Further it can be observed the rate of decrease in absorbance is great in the case of films doped with 8%. The decreasing of the absorbance band (MO) at 460 nm, (MB) at 660 nm and (MV) at 560 nm is very remarkable suggesting high photoreactivity. However, in our experiment, all the thin films doped with Fe showed noticeable increased photodegradation compared with pure ZnO. Fig. 9 showed that the 8 % Fe-doped catalyst has higher values of photocatalytic activity than of the 2%, 4% and 6% Fe-doped thin films catalysts, and required only 60 min to decompose in aqueous solution. This can be related to the many reasons: (1) due to higher specific surface area, surface morphology, crystal structure and the enhanced photoresponse of the films. The film doped with 8 % had higher surface roughness (surface roughness = 3.24 nm compared with 0.98, 2.98, 2.92, and 2.72 nm of the film doped with 0%, 2%, 4%, and 6% respectively). The effective surface area increases with increase the surface roughness which in turn improved the photodegradation [32]. (2) Introducing Fe in the ZnO lattice leads to increased absorption in the UV light range [4, 7] (as shown by reducing energy band gap). Therefore, the electronic interaction between Fe species and ZnO leads to the visible light photocatalytic activity of zinc oxide thin films. Where, the formation dopant energy levels of iron in the energy band gap of zinc oxide leads to the change in energy band gap [33]. The oxidation activity of ZnO photocatalyst thin films is enhanced, when the oxidation-reduction potential of the electrons and holes is increased [34].

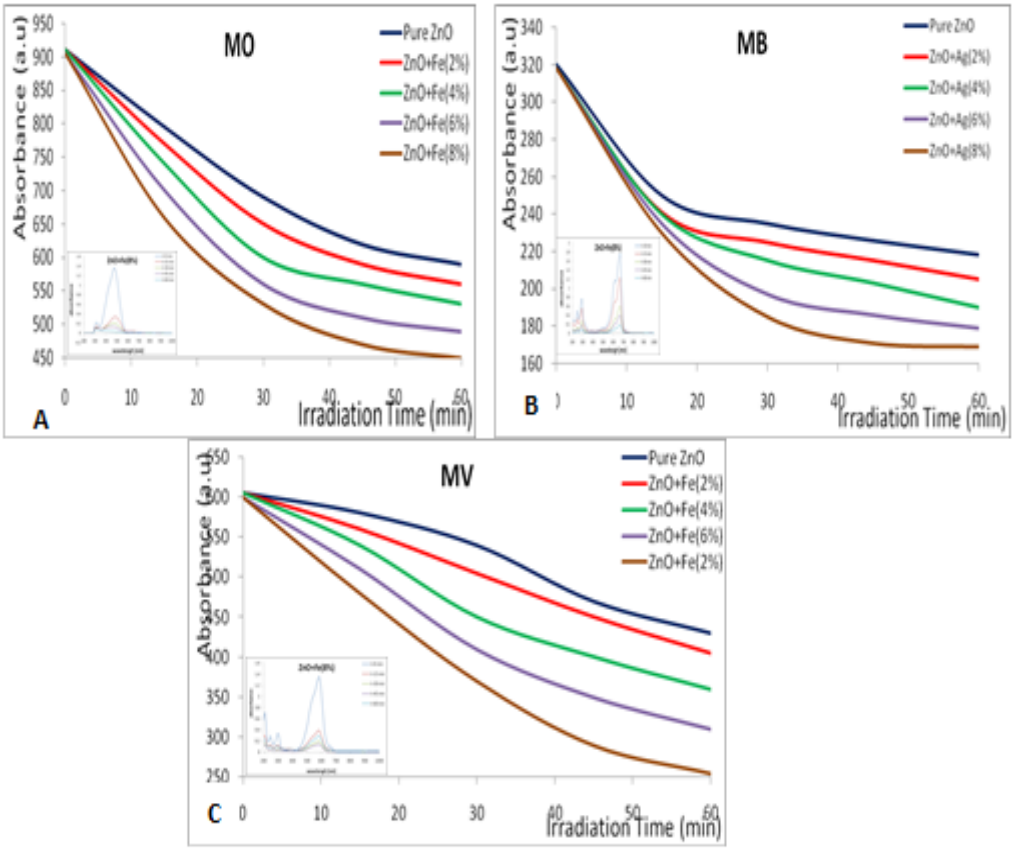

Fig. 9: Absorbance of an aqueous solution with irradiation time of the ZnO films immersed in it. (A) for methyl orange (MO). (B) methyl blue (MB). (C) methyl violet (MV). Inset: absorption spectra of aqueous solution (100 mg/l) degraded by a ZnO film.

The photocatalytic degradation can be calculating by using the relation [35].

$$\text{Ln } C/ C_0 = -k\, t \qquad (4)$$

where C is the concentration of MB, MO and MV (mg/l) at each interval of time in mg/l, C_0 is the initial concentration, t is the irradiation time in minutes and k is the rate constant.

The degradation (%) can be calculated using the relation [35]:

$$\text{Degradation (\%)} = (C_0\text{-}C/ C) \times 100 \qquad (5)$$

The photocatalytic activity of the different zinc oxide samples was estimated by calculating the rate constant (k values) from the slope of the diagram in Fig. 10. The k values and the degradation (%) of MO, MB and MV (Fig.11) exhibiting the photocatalytic activity of zinc oxide thin films are given in Table 2.

One can conclude that the surface morphology of sol-gel films, energy gap and the crystallites sizes have effect on the photocatalytic activity of the thin films. The results exhibited the higher photocatalytic activity can obtained by significantly advanced surface. Thin films with Fe doping are hopeful and efficient catalysts for the decomposition of organic pollutants by photocatalytic oxidation.

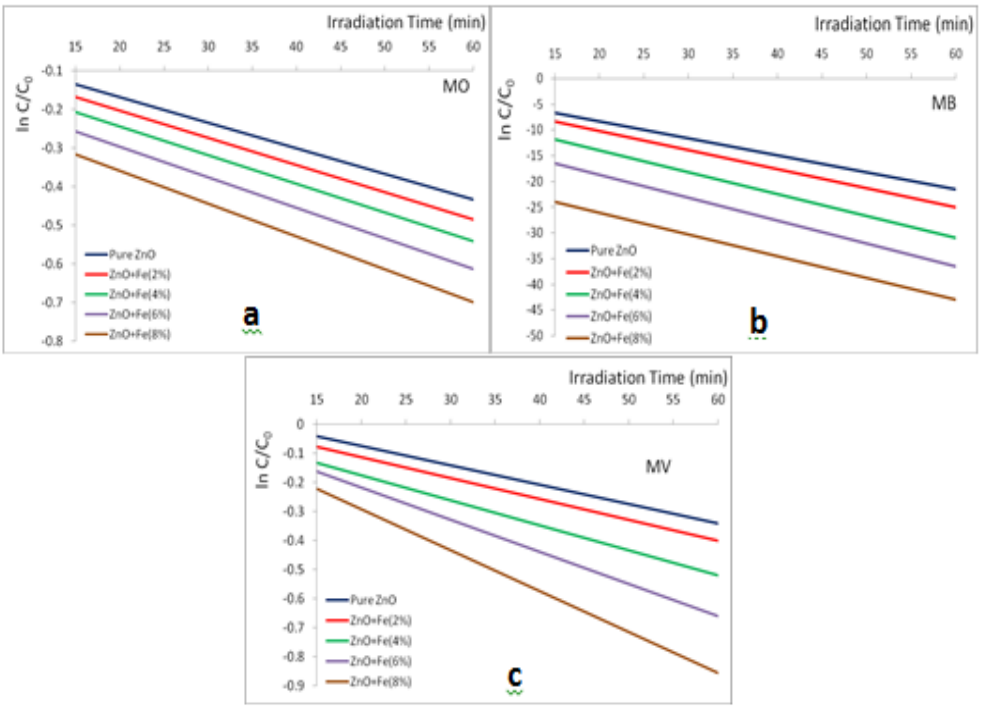

Fig.10: The relation between ln C /C_0 with irradiation time for zinc oxide thin films. (a) MO, (b) MB and (c) MV solution.

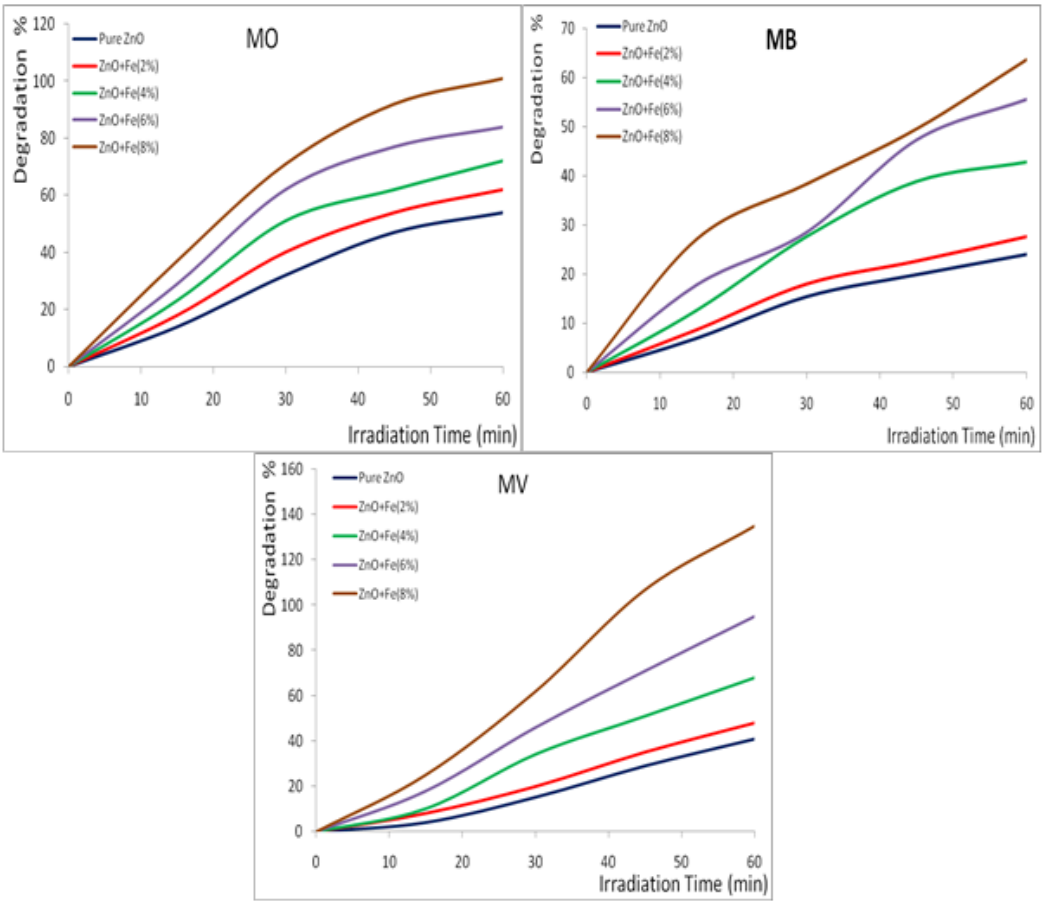

Fig.11: Degradation of aqueous MO, MB and MV solution as a function of irradiation light time of the ZnO thin films immersed in it.

Table 2: Illustrate the rate constant (k) and degradation (%) of the (a) MO, (b) MB and (c) MV (100 mg/l) solution.

samples	K min^{-1} for MO	Degradation in 60 min	K min^{-1} for MB	Degradation in 60 min	K min^{-1} for MV	Degradation in 60 min
Pure ZnO	0.0072	54	0.00358	24	0.0057	41
2% Fe	0.0081	62	0.00405	28	0.00669	48
4% Fe	0.009	72	0.0051	43	0.00865	68
6% Fe	0.0102	84	0.00607	56	0.011	95
8% Fe	0.0116	101	0.0071	64	0.0143	135

Conclusions

ZnO:Fe thin films were prepared through simple and low cost spin-coating sol-gel method. The deposited film was 300 nm thick, and XRD studies of as-deposited samples show polycrystalline structure with hexagonal wurtzite structure of ZnO and Fe:ZnO thin films. With Fe doping from 0–8 wt. %, the prepared film has energy band gap of approximately 3.75 eV to 3.3 eV. It was found that Fe concentration affect surface roughness, grain size, absorption of UV light and photocatalytic activity of the samples. The photocatalytic activity of the samples was enhanced by all these factors. The optimum concentration of iron under UV light is 8%, degradation process with irradiation time UV light for 60 min. Moreover, the photocatalytic activity of thin films against which indicates the photodegradation of MO, MB and MV under UV light irradiation (354 nm, 6 W) has been developed in this research.

References

[1] R. Ahlawat, V. C. Srivastava, I. D. Mall, S. Sinha, Clean: Soil, Air, Water, 36 (2008) 863-869.

[2] Y. Jin, J. Wang, B. Sun, JC. Blakesley, N.C. Greenham, Nano Letters, 8, 6 (2008) 1649-1653.

[3] J. Wang, P. Liu, X. Fu, Z. Li, W. Han, X. Wang, Langmuir, 25 (2008) 1218-1223.

[4] Y. Lv, C. Pan, X. Ma, R. Zong, X. Bai, Y. Zhu, Appl. Catal., B 138 (2013) 26-32.

[5] Y. Lv, Y. Zhu, Y. Zhu, J. Phys. Chem., C 117 (2013) 18520-18528.

[6] J. Wang, Z. Wang, B. Huang, Y. Ma, Y. Liu, X. Qin, X. Zhang, Y. Dai, ACS Appl. Mater. Interfaces, 4 (2012) 4024-4030.

[7] A. Naldoni, M. Allieta, S. Santangelo, M. Marelli, F. Fabbri, S. Cappelli, C. L. Bianchi, R. Psaro, V. Dal Santo, J. Am. Chem. Soc., 134 (2012) 7600-7603.

[8] M. Kong, Y.Li, X. Chen, T. Tian, P. Fang, F. Zheng, X. Zhao, J. Am. Chem. Soc., 133 (2011) 16414-16417.

[9] Y. Zheng, C. Chen, Y. Zhan, X. Lin, Q. Zheng, K. Wei, J. Zhu, Y. Zhu, Inorg. Chem., 46 (2007) 6675-6682.

[10] M.S. Rad, A. Kompany, AK. Zak, M. Javidi, S. Mortazavi, J. Nanopart. Res., 15 (2013) 1-8.

[11] B. Li, T. Liu, Y. Wang, Z. Wang, Journal of Colloid and Interface Science, 377, 1 (2012) 114-121.

[21] K. Ueda, H. Tabata, T. Kawai, Applied Physics Letters, 79, 7 (2001) 988-990.

[13] B. Liu, H.C. Zeng, Journal of the American Chemical Society, 125, 15 (2003) 4430-4431.

[14] L. Spanhel, M.A. Anderson, Journal of the American Chemical Society, 113, 8 (1991) 2826-2833.
[15] X. Liu, X. Wu, H. Cao, R. Chang, Journal of Applied Physics, 95, 6 (2004) 3141-3147.
[16] P. Carcia, R. McLean, M. Reilly, GN. J.r, Applied Physics Letters, 82, 7 (2003) 1117-1119.
[17] P. Singh, K. Mondal, A. Sharma, Journal of Colloid and Interface Science, 394 (2013) 208-215.
[18] E.A. Meulenkamp, Journal of Physical Chemistry B 102, 29 (1998) 5566-5572.
[19] S.M.H. AL-Jawad, Optik, 146 (2017) 17-26.
[20] B. Cullity and S. Stock, "Elements of X-Ray Diffraction", Pearson Prentice Hall, New Jersey, (2001).
[21] N. Mahmoudi Khatir, Z. Abdul-Malek, A. Khorsand Zak, J. Sol-Gel Sci. Technol., 78 (2016) 91-98.
[22] R. Yousefi, Zak AK, F. Jamali-Sheini, Ceram Int., 39 (2013) 1371-1377.
[23] C. Wang, Z. Chen, Y. He, Appl. Surf. Sci., 255, 15 (2009) 6881-6887.
[24] S. M. Salaken, E. Farzana, J. Podder, Journal of Semiconductors, 34, 7 (2013) 1-6.
[25] B.D. Cullity, SR. Stock, Elements of X-ray diffraction. Prentice Hall, Upper Saddle River, (2001).
[26] K. J. Kim, Y. R. Park, J. Appl. Phys., 96, 8 (2004) 4150-4153.
[27] L. Xu, X. Li, J. Cryst, Growth, 312 (2010) 851-855.
[28] S.M. H. AL-Jawad, M. R. Mohammad, N. Jamal Imran, Surface Review and Letters, 25, 6 (2018) 16.
[29] S. Y. Al Dabagh and E. E. Makhool, IOSR Journal of Dental and Medical Sciences, 1, 15 (2016) 54-60.
[30] N. Talebian, M. Reza Nilforoushan, R. Ramazan Ghasem, J. Sol-Gel Sci. Technol., 64 (2012) 36-46.
[31] J. Weizhong, W. Ying, Gu. Lixia, Journal of Non-Crystalline Solids, 353 (2007) 4191-4194.
[32] G. Zheng, W. Shang, L. Xu, S. Guo, Z. Zhou, Materials Letters 150 (2015) 1-4.
[34] B. Q.Wang, C. H. Xia, J. Iqbal, N. J. Tang, Z. R. Sun, Y. Lv, L. Wu, Solid State Sci., 11 (2009) 1419-1422.
[34] M. Y. Guo, A. M. C.Ng, F. Liu, A. B. Djurisič , W. K. Chan, H. Su, K. S. Wong, J. Phys. Chem., C 115 (2011) 11095-11101.
[35] J. Yu, X. Zhao, Q. Zhao, Materials Chemistry and Physics, 69 (2001) 25-29.